

Nanoscale clusters in the high performance thermoelectric $\text{AgPb}_m\text{SbTe}_{m+2}$

H. Lin, E. S. Božin, S. J. L. Billinge

Department of Physics and Astronomy, Michigan State University, East Lansing, MI 48824

Eric Quarez, M. G. Kanatzidis

*Department of Chemistry, Michigan State University, East Lansing, MI 48824**

(Dated: October 30, 2018)

The local structure of the $\text{AgPb}_m\text{SbTe}_{m+2}$ series of thermoelectric materials has been studied using the atomic pair distribution function (PDF) method. Three candidate-models were attempted for the structure of this class of materials using either a one-phase or a two-phase modeling procedure. Combining modeling the PDF with HRTEM data we show that $\text{AgPb}_m\text{SbTe}_{m+2}$ contains nanoscale inclusions with composition close to $\text{AgPb}_3\text{SbTe}_5$ randomly embedded in a PbTe matrix.

PACS numbers: 61.10.-i, 72.15.Jf, 73.50.Lw, 73.63.Bd

I. INTRODUCTION

Compounds in the series based on composition $\text{AgPb}_m\text{SbTe}_{m+2}$ can exhibit exceptional thermoelectric properties.¹ They are promising for electrical power generation and in the temperature range 600 to 900 kelvin, they are expected to significantly outperform all other reported bulk thermoelectric systems. The dimensionless thermoelectric figure of merit, ZT ,² of the $m \sim 18$ composition material was found to reach 1.7 at 700 kelvin, compared to the highest observed ZT of only 0.84 for PbTe at 648 kelvin in n-doped material.^{3,4} This is a surprisingly large enhancement in ZT for the addition of just 10% per formula-unit of silver and antimony ions. It is clearly of the greatest importance to trace the origin of the ZT enhancement.

High resolution transmission electron microscopy (HRTEM) images from these materials indicate the presence of nanosized domains of a Ag-Sb-rich phase endotaxially embedded in the PbTe matrix.⁵ An interesting possibility is that these nanoclusters are key components in the ZT enhancement. The HRTEM images show the clusters are randomly distributed through the matrix and are not long-range ordered. Randomly distributed nanoscale clusters which strain the lattice might be expected to increase phonon scattering and reduce the thermal conductivity which would enhance ZT provided the electrical conductivity was not degraded to a greater degree. An additional enhancement in ZT is possible if the material has an increased electronic density of states (DOS) at the Fermi-level, E_f . A recent theoretical analysis showed that resonant structures form in the DOS near E_f in the presence of ordered Ag and Sb atoms in the matrix and in the nanoclusters observed in HRTEM.^{6,7} The calculations used gradient corrected density functional theory and assumed different structural models for the clusters, since details of their structure and chemical ordering are not known. This type of DOS resembles that of the “best thermoelectric material” predicted earlier.^{7,8}

The composition and atomic arrangements within the nanoclusters is a challenging topic since the clusters are

not periodically long-range ordered. They are dispersed inside a matrix and cannot be studied crystallographically. A probing method sensitive to local structure is needed such as the atomic pair distribution function (PDF) analysis of x-ray powder diffraction data.⁹ In the past decade the PDF technique has emerged as a powerful tool for obtaining local structural information from complex materials.^{9,10} It is a total scattering method that takes into account both Bragg and diffuse scattering information and gives structural information in real space on various length scales. Recently, it was successfully used to study chemical short-range ordered clusters randomly embedded in a parent matrix,¹¹ in analogy with the present situation. Here we report a PDF study of a series of compounds in the $\text{AgPb}_m\text{SbTe}_{m+2}$ series with $m = 6, 12$ and 18. For comparison we also studied the end member compound, PbTe the $m = \infty$ member of the series. The resulting PDFs have sufficiently high quality to see a structural signature of the nanoclusters, even in the PbTe-rich $m = 18$ compound. These differences were sufficiently large to allow different models of the local structure to be differentiated, confirming the existence of the clusters in the bulk, and narrowing down their composition and the atomic arrangement in the clusters.

II. EXPERIMENTAL DETAILS

A. Sample Preparation

Ingots with nominal compositions $\text{AgPb}_6\text{SbTe}_8$, $\text{AgPb}_{12}\text{SbTe}_{14}$ and $\text{Ag}_{0.86}\text{Pb}_{18}\text{SbTe}_{20}$ were synthesized by annealing, in quartz tubes under vacuum, mixtures of Ag, Pb, Sb, and Te elements at 1000 °C for 8 h. This was followed by a fast cooling to 850 °C for 1 h, slow cooling to 800 °C for 12 h, and then cooling to 400 °C for 12 h. This method of cooling produces more consistent samples.

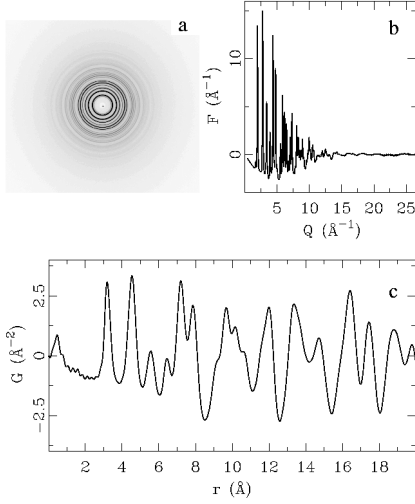


FIG. 1: (a) The raw data diffraction pattern observed on the image plate. (b) $F(Q)$ and (c) $G(r)$ for the $\text{Ag}_{0.86}\text{Pb}_{18}\text{SbTe}_{20}$ sample. In the Fourier transform, Q_{max} was set to 26.5 \AA^{-1} .

B. High energy x-ray diffraction experiments

X-ray diffraction measurements were made on the $\text{AgPb}_m\text{SbTe}_{m+2}$ series of materials with $m = 6, 12, 18$ and ∞ at room temperature using the recently developed rapid acquisition pair distribution function (RAPDF) approach¹² at the MU-CAT 6-ID-D beam-line at the Advanced Photon Source (APS) at Argonne National Laboratory.

X-ray powder diffraction samples were prepared by carefully grinding the compounds in a mortar and pestle and sieving through a 400-mesh sieve. The powders were packed into hollow flat aluminum plate sample containers with a radius of 0.25 cm and thickness of 1.0 mm, sealed between thin Kapton films.

The x-ray energy used was 87.005 keV ($\lambda = 0.14248 \text{ \AA}$). The data were collected using a circular image plate (IP) camera Mar345, 345 mm in diameter. The camera was mounted orthogonally to the beam path with a sample-to-detector distance of 208.86 mm which was determined by calibrating with a silicon standard sample.¹²

In order to avoid saturation of the detector, each measurement was carried out by multiple exposure to the x-rays. Each exposure lasted 10 seconds, and each sample was exposed five times to improve the counting statistics. An example of the raw data on the image plate is shown in Fig. 1(a). All raw 2D data were integrated and converted to intensity versus 2θ format using the Fit2D program package,¹³ where 2θ is the angle between the incident and scattered x-rays. Data sets for the same sample were combined using the same program. Data for

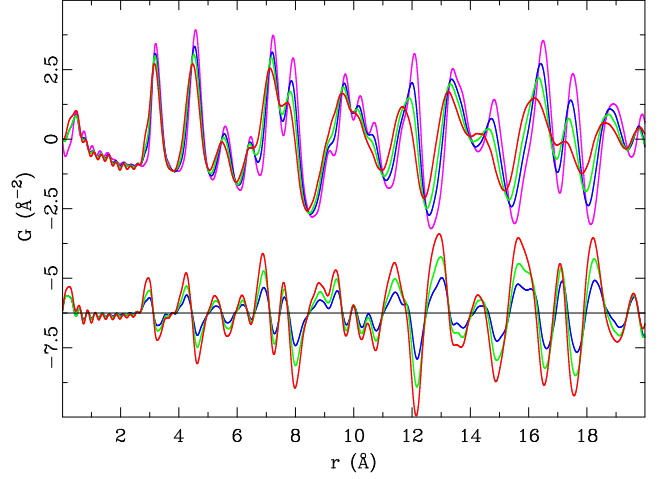


FIG. 2: $G(r)$ and $DG(r)$ (compared to PbTe) for samples with different m value. Magenta curve is for PbTe, blue curves are for sample $\text{Ag}_{0.86}\text{Pb}_{18}\text{SbTe}_{20}$, green for sample $\text{AgPb}_{12}\text{SbTe}_{14}$, red for $\text{AgPb}_6\text{SbTe}_8$.

the empty container were also collected and subtracted from the sample data during the correction step. Standard corrections for multiple scattering, polarization, absorption, Compton scattering and Laue diffuse scattering were applied to the integrated data to obtain the reduced total structure function $F(Q)$, as described in detail in Refs. [9,12]. Data correction and processing utilized the PDFgetX2 program package.¹⁴ An example of the $F(Q)$ for the $m = 18$ sample is shown in Fig. 1. Sine Fourier transformation of $F(Q)$ gives the atomic PDF, $G(r)$, according to $G(r) = \frac{2}{\pi} \int_{Q_{min}}^{Q_{max}} F(Q) \sin(Qr) dQ$, where Q is the magnitude of the scattering vector. The good statistics in the high- Q region of the data (Fig. 1(b)) allowed a $Q_{max} = 26.5 \text{ \AA}^{-1}$ to be used which gives high-quality PDFs with good resolution. This is evident in Fig. 1(c) where $G(r)$ is plotted for the sample $\text{Ag}_{0.86}\text{Pb}_{18}\text{SbTe}_{20}$.

The $G(r)$ data for all samples are plotted in Fig. 2 on top of each other. The difference curves plotted below are the differences between the different m -value PDFs and pure PbTe. The difference curves show fluctuations that are much larger than the estimated random errors on the data and therefore have a real origin, encoding the local structural differences between the $\text{AgPb}_m\text{SbTe}_{m+2}$ and PbTe compounds. The fluctuations in the difference curves are highly correlated between the different m -values, growing in amplitude from $m = 18, 12$ to 6, as expected. This suggests that the local structures in each case are similar and gives some confidence that the results from lower m -value compounds can give insight about higher m -members. It also gives us confidence that the smaller ripples in the difference curve from the $m = 18$ compound have a real structural origin.

C. Modeling

Structural information was extracted from the PDFs using a full-profile real-space local-structure refinement method¹⁵ analogous to Rietveld refinement.¹⁶ We used an updated version¹⁷ of the program PDFFIT¹⁸ to fit the experimental PDFs. PDFFIT allows for multiple data-sets to be refined and can also handle multiple phases. Starting from a given structure model and given a set of parameters to be refined, PDFFIT searches for the best structure that is consistent with the experimental PDF data. The residual function (Rw) is used to quantify the agreement of the calculated PDF from model to experimental data:

$$Rw = \sqrt{\frac{\sum_{i=1}^N \omega(r_i) [G_{obs}(r_i) - G_{calc}(r_i)]^2}{\sum_{i=1}^N \omega(r_i) G_{obs}^2(r_i)}} \quad (1)$$

Here the weight $\omega(r_i)$ is set to unity.

In this modeling we took advantage of the ability to refine multiple phases in PDFFIT. We searched for domains of Ag and Sb rich material embedded in the PbTe matrix. Provided we fit the PDF over a range of r that is much less than the particle diameter, it is a good approximation to model the data as being made up of two distinct phases. This neglects cross-terms; i.e., atom pairs where one atom is in one phase and the neighboring atom is in the other phase. However, our experience suggests that these terms are small and a reasonable and simple starting point is to neglect these terms and model the phases as distinct (i.e., incoherent). The HRTEM images suggest that the nano-cluster domains have diameters of the order of a few nanometers and our fitting is carried out over a range up to 20 Å. Thus, some inconsistencies in the fits in the high- r range should be attributable to the neglected cross-terms. This approximation can be removed in the future, but only at the expense of having to fit the data with very large models. The success of the current modeling seems to suggest that this is not warranted at this point.

In PDFFIT, each phase in the multi-phase mixture has its own scale-factor that is refined. This scale factor reflects both the relative phase-fraction of the phases, but also any differences in the scattering power of the two phases, which depends on the respective compositions of the phases. Here we present the equations that allow us to extract phase fractions from the refined scale factors of the phases. In PDFFIT, the total PDF $G(r)$ is defined as a summation of the different phases as follows:

$$G'_s(r_k) = f_s B_s(r_k) \sum_{p=1}^P f_p G_p^s(r_k), \quad (2)$$

where f_s is the overall scale factor and B_s is an experimental resolution factor for data set s . The sum is over the different structural phases, p , in a multiphase refinement and $G_p(r_k, s)$ is the model PDF for a single phase p . The weighted abundance of each phase is given

by $f_p = \frac{\langle b_p \rangle^2}{\langle b \rangle^2} \frac{N_p}{N}$ where $\langle b_p \rangle$ and $\langle b \rangle$ are the averaged scattering factors for phase p and the whole sample, respectively, and N_p and N are the total atom number for phase p and the whole sample. We can easily calculate $\frac{N_p}{N}$ from the stoichiometry of phase p and the whole sample. After refinement we extract $\frac{N_p}{N}$ from the weighted scale factor and then compare it to the calculated one to see whether the refinement result is self-consistent with the known stoichiometry. For example, let's suppose we use two phases PbTe and $\text{AgPb}_x\text{SbTe}_{x+2}$ to model $\text{AgPb}_m\text{SbTe}_{m+2}$. We can set up the following two equations to get $\frac{N_{\text{PbTe}}}{N}$ and $\frac{N_x}{N}$:

$$\frac{N_x}{2x+4} = \frac{xN_x}{m(2x+4)} + \frac{N_{\text{PbTe}}}{2m}, \quad (3)$$

and

$$N_x + N_{\text{PbTe}} = N. \quad (4)$$

Since x and m are known we can extract the expected ratio $\frac{N_p}{N}$ for comparison with the value obtained from the refinement.

To test this procedure, we used a sample made by mechanically mixing PbTe and AgSbTe_2 powders with atom number ratio of 1:3 and carried out a two-phase refinement. The refined value of $\frac{N_p}{N}$ was 0.69 compared to the expected values of 0.75. This suggests that we can obtain the phase fractions to an accuracy at the 10% level.

Each data-set (for the finite- m cases) was modeled with a sequence of models. Model H is a single phase homogeneous model of the correct average composition. Models $NC0_n$, $NC1_n$, $NC2_n$, $NC3_n$ and $NC4_n$ are two-phase models that test for the presence and nature of nanoscale clusters in the material ('NC' refers to nano-cluster). In all the NC models, the first phase is always a pure PbTe component. The second phase comes from the embedded nanoclusters where we have tried different models varying their composition and chemical ordering. The number after the NC, '0', '1', '2', '3' or '4', refers to the increasing Pb component in the second phase as will be explained in more detail later. The integer index n refers to a different chemically ordered variant of each nanocluster model, where n increases when the chemical ordering in the special variant increases.

In solid solution model H, one homogeneous phase is defined in which the dopant Ag, Sb atoms randomly occupy the Pb sublattice. The cubic symmetry of the PbTe matrix is retained, and thus only one lattice parameter is refined. These models have four refinable structural parameters and two experimental parameters for a total of six refinable parameters. The PbTe structure is shown in Fig. 3(a).

In the case of $NC0_n$, a two-phase model is applied. The major phase is still PbTe. The chemical component of the second phase is the same as bulk AgSbTe_2 .¹⁹ In this model there are no Pb atoms inside the minor phase. For the minor phase of this model we tried both

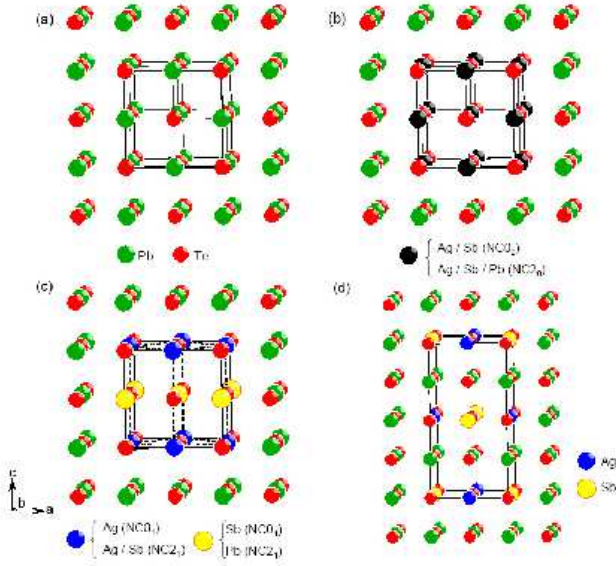


FIG. 3: The unit cells for different models are shown here. (a) is the PbTe major phase. In all plots Te is shown as red atoms and Pb as green. (b) Chemically disordered AgSbTe₂ in $NC0_1$ and chemically disordered AgPb₂SbTe₄ in $NC2_0$. (c) Chemically ordered AgSbTe₂ in $NC0_1$ and partially chemically disordered AgPb₂SbTe₄ in $NC2_1$. (d) Chemically ordered AgPb₂SbTe₄ in model $NC2_2$ resulting in 2-fold supercell along one crystal axis. In all models the Te (red) sublattice is not changed.

a chemically disordered cluster model $NC0_0$ with a cubic unit cell and Ag, Sb atoms distributed randomly on the lead sublattice (Fig. 3(b)) and a tetragonal unit cell with Ag and Sb atoms chemically ordered on the Pb sublattice sites ($NC0_1$, Fig. 3(c)). These models have nine and eleven structural parameters, respectively, resulting in eleven and thirteen total refinable parameters.

The model $NC2_n$ also contains two phases, the major phase is still PbTe while the minor phase contains atoms with the chemical composition of AgPb₂SbTe₄. In this model, we also tried various possible chemical ordering possibilities for the minor phases, which can be totally chemically ordered ($NC2_2$), partially chemically ordered ($NC2_1$) and totally chemically disordered ($NC2_0$). In the totally chemically ordered case, the unit cell contains 16 atoms forming 4 layers as shown in Fig. 3(d). There are two types of layer. Ag, Sb and Te atoms form one type of layer and Pb, Te atoms form the second type. The two types of layer intersect with each other. The two lattice parameters in the plane of the layer are the same, but the lattice parameter in the perpendicular direction is approximately doubled. The resulting symmetry is refined as tetragonal. This model has twelve structural parameters and fourteen total refinable parameters. In the $NC2_1$ variant, Ag and Sb atoms distribute randomly in their plane but do not substitute on the Pb or Te sites (Fig. 3(c)). In the $NC2_0$ case, (Fig. 3(b)) Pb, Sb and

Ag atoms distribute randomly on the metal sublattice of the whole minor phase resulting in a cubic structure. In both of the two latter cases, there are only eight atoms in the unit cell. These models have eleven and nine structural, and thirteen and eleven total refinable parameters, respectively.

Models $NC1_0$, $NC3_0$ and $NC4_0$ are almost the same as model $NC2_0$ except that the chemical compositions of the minor phase are AgPbSbTe₃, AgPb₃SbTe₅ and AgPb₄SbTe₆, respectively. The modeling of the different $NC2_n$ models indicated that the PDF was not sensitive to the degree of chemical ordering in the minor phase and the results for chemically ordered or partially ordered cases of models $NC1_n$, $NC3_n$ and $NC4_n$ are not presented here.

All refinements were performed over the range of PDF from 2.85 Å to 20 Å. The PbTe end member compound was fit with a homogeneous model H and two-phase models $NC1_n$ and $NC2_n$. All models were fit to the $m = 6$, 12 and 18 datasets.

III. RESULTS

First we consider the the pure PbTe end-member compound. The homogeneous model H, as expected, fit reasonably well resulting in an $Rw = 0.086$. Displacement parameters, U_{iso} , for Te and Pb atoms are 0.013 Å² and 0.029 Å² respectively and the lattice parameter is 6.47 Å. Refining the two-phase model $NC0_n$ and $NC2_n$ to the PbTe data did not result in an improvement in Rw despite the greater number of parameters. The scale factor for the second, non-physical, phase becomes very small (smaller than 0.3 percent), and the displacement parameters in this phase also become very large, indicating that the fit is attempting to eliminate the second phase. The result from the two phase refinement shows that the PDF is able to distinguish single from two-phase behavior.

We now turn our attention to the $m = 6$ compound that has the largest volume fraction of second phase in it. First this was fit with the homogeneous model H. The fit is poor as shown in Fig. 4(a), with $Rw = 0.212$. Significantly better fits were obtained from the two-phase models (Table I and Fig. 4(b)) with $Rw = 0.0724$ from the chemically disordered model $NC2_0$. The refined values are shown in Table I. Similar results were obtained from the chemically disordered models. This analysis strongly suggests that the Ag and Sb clusters are present in the bulk of the material and are not an artifact of the TEM measurement.

We now wish to differentiate between the different composition two-phase models $NC0_n$ – $NC4_n$. In terms of fit to the data and Rw , all four models performed comparably well, both in the chemically ordered and disordered states. The refined parameters that produce these good fits allow us to differentiate somewhat between the models. In particular, the refined phase fractions for the two phase refinements can be compared with the values

TABLE I: Results from PDFFIT for the $\text{AgPb}_6\text{SbTe}_8$ sample. $n = \frac{N_{\text{PbTe}}}{N}$ is the ratio of atom numbers in PbTe phase to whole sample, n_0 is the expected ratio calculated from the chemical stoichiometry (see text for details). U_{atom} are the displacement parameters for atoms on different sites.

		model H	$NC0_0$	$NC0_1$	$NC1_0$	$NC2_0$	$NC2_1$	$NC2_2$	$NC3_0$	$NC4_0$
PbTe	R_w	0.22	0.066	0.065	0.070	0.072	0.070	0.075	0.070	0.071
	n/n_0	—	0.276/0.750	0.257/0.75	0.321/0.625	0.358/0.500	0.383/0.500	0.372/0.500	0.376/0.325	0.404/0.250
	a	—	6.41	6.41	6.41	6.41	6.41	6.41	6.41	6.41
	U_{Te}	—	0.0291	0.0255	0.0299	0.0285	0.0305	0.0297	0.0299	0.0299
	U_{Pb}	—	0.0295	0.0307	0.0297	0.0320	0.0298	0.0311	0.0294	0.0293
Phase 2	a	6.33	6.22	6.21	6.22	6.22	6.23	6.226	6.219	6.220
	c	—	—	6.24	—	—	6.19	12.40	—	—
	U_{Te}	0.080	0.0480	0.0488	0.0415	0.0704	0.0409	0.0325	0.0384	0.0377
	U_{Pb}	0.061	—	—	0.08444	0.0550	0.0852	0.0875	0.08724	0.0879
	U_{Ag}	0.061	0.0782	0.0382	0.0844	0.0550	0.0852	0.0875	0.08724	0.0879
	U_{Sb}	0.061	0.0782	0.203	0.0844	0.0550	0.0852	0.0875	0.0872	0.0879

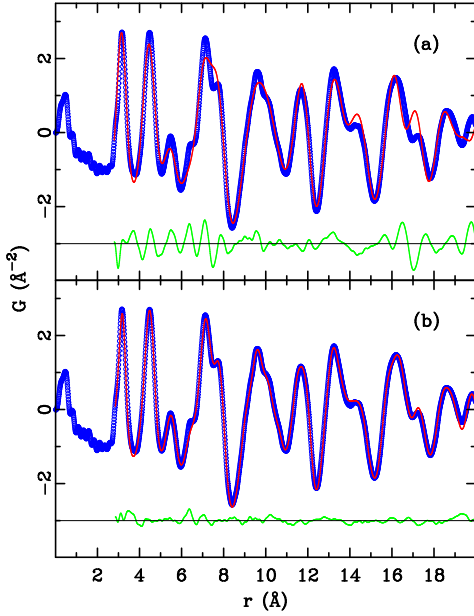


FIG. 4: (a) PDF from the homogeneous H model for sample $\text{AgPb}_6\text{SbTe}_8$. The line with empty circles is the data, the solid line is the calculated curve from the fitting and the line offset below is their difference. (b) Chemically disordered case of model $NC2_0$ for $\text{AgPb}_6\text{SbTe}_8$. Line attributions are the same as in (a).

that should be obtained based on the overall chemical composition of the material. As can be seen in Table I, the $NC0_n$ and $NC1_n$ models significantly underestimate, and $NC4_n$ significantly overestimates, the phase fraction. The $NC2_n$ and $NC3_n$ compositions give phase fractions much closer to those expected stoichiometrically, with $NC3_n$ giving the best agreement. This is strong evidence that the nanoclusters contain significant amounts of Pb atoms and are not pure $\text{AgPb}_6\text{SbTe}_8$.

The refinements suggest that the average composition of the nanoclusters is “ $\text{AgPb}_3\text{SbTe}_5$ ”. However, it is unlikely that the real clusters have this composition since it is not possible to construct an ordered model with this

composition by interleaving Ag/Sb and Pb layers on the Pb sublattice; it is necessary to have a layer with Ag/Sb mixed with Pb. As we discuss below, this is not expected on theoretical grounds. It could come about due to the presence of anti-phase boundaries between Pb regions and Ag/Sb regions, in analogy with the Na_3BiO_4 material studied previously¹¹, though it seems unlikely that this can occur within an individual nanocluster. From this point of view, it seems more likely that clusters with compositions of $\text{AgPb}_2\text{SbTe}_4$ and $\text{AgPb}_4\text{SbTe}_6$ coexist in the matrix yielding, on average, the observed “ $\text{AgPb}_3\text{SbTe}_5$ ” composition. It should also be noted that some uncertainty exists in the two-phase modeling, especially taking into account the fact that we are modeling coherently embedded nanoclusters approximated as an incoherent mixture. The strong result is that significant Pb content exists in the nanoclusters but there is probably some uncertainty on the precise value.

We investigated the chemical ordering within the nanoclusters by focusing on the $NC2_n$ model that lends itself to rational chemically ordered models. Refinements of the chemically disordered and partially ordered variants of models $NC2_n$ yielded comparable fits to the chemically ordered fits, with comparable values of refined parameters (Table I) suggesting that the current PDF measurements alone are not sensitive enough to differentiate the chemical ordering within the minor phase.

Finally, we note that similar results were obtained when the $m = 12$ and $m = 18$ samples were refined in the same way. The results for the chemically disordered “ $\text{AgPb}_3\text{SbTe}_5$ ” model are presented in Table II. The refined phase fractions nicely track the nominal composition giving us good confidence that the two-phase modeling is giving physically meaningful results and that nanoclusters of average composition close to $\text{AgPb}_3\text{SbTe}_5$ are present.

TABLE II: Results from model $NC3_0$ for three different m -members. $n = \frac{N_{PbTe}}{N}$ is the ratio of atom numbers in the PbTe phase to whole sample, n_0 is the expected ratio calculated from chemical stoichiometry. U_{atom} is the thermal factor for atoms on different site.

		AgPb ₆ SbTe ₈	AgPb ₁₂ SbTe ₁₄	Ag _{0.86} Pb ₁₈ SbTe ₂₀	PbTe
PbTe	R_w	0.072	0.066	0.074	0.086
	n/n_0	0.376/0.325	0.571/0.643	0.693/0.750	-
	a	6.41	6.43	6.45	6.47
	U_{Te}	0.029	0.0246	0.0214	0.013
	U_{Pb}	0.032	0.0280	0.0262	0.029
Phase 2	a	6.22	6.26	6.29	-
	U_{Te}	0.0371	0.0779	0.0826	-
	U_{Pb}	0.0815	0.0876	0.0691	-
	U_{Ag}	0.0815	0.0876	0.0691	-
	U_{Sb}	0.0815	0.0876	0.0691	-

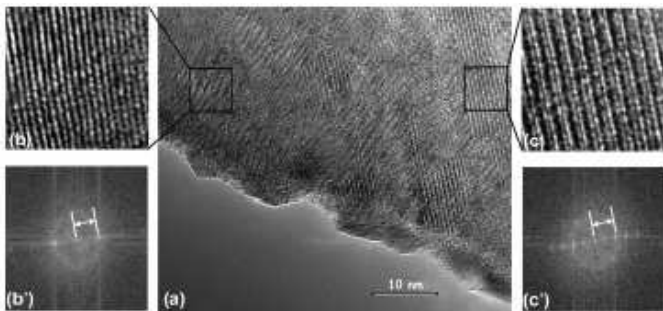


FIG. 5: A HRTEM image of a region of a sample of $Ag_{0.86}Pb_{18}SbTe_{20}$. The four smaller pictures at the side are the amplified pictures for different (lattice) local region and their fourier transformed images.

IV. DISCUSSION

The success of models $NC2_n$ and $NC3_n$ verify that the TEM observations of nanoclusters reflect a bulk average property of this material. These models also provide evidence for the chemical composition of the minor phase and give a hint to the chemical distribution of Ag, Sb and Pb atoms in the minor phase, although little information is available about the degree of chemical ordering.

In Fig. 5 we show a HRTEM image that suggests that clusters are present that result in a doubling of the lattice parameter in the second phase, though not all clusters show this behavior. This is consistent with the partially or fully ordered model $NC2_n$ variants, $n = 1, 2$, which alternate Pb and Ag/Sb layers on the metallic sublattice. The fully chemically ordered case in model $NC2_2$ was found to be the stable configuration in a coulomb lattice-gas Monte Carlo simulation study of the ground state of this system as a function of m .²⁰ Thus, we believe that clusters with the totally chemically ordered form in model $NC2_2$ (Fig. 3(d)) are present as nanoclusters in the large m compounds. This may not be the unique form of the nanoclusters, and indeed, not all the nanoclusters evident in the TEM images show this cell doubling. They presumably form by a nano-phase separation

of constituents accompanied by an imperfect and defective ordering and there appears to be considerable spatial disorder of the chemical constituents; though the nanoclusters are coherently endotaxially embedded in the matrix, they are not well ordered. Incorporating more Pb in the nanoclusters allows the system to balance its desire to phase separate, with maintaining a degree of lattice matching to keep the nanoparticles embedded in the matrix without incoherent interfaces. The refined lattice parameters for the nanocluster phases are smaller than the matrix: 6.23-6.29 Å compared to 6.41 Å for the strained matrix and 6.47 Å for relaxed PbTe. Both the chemical inhomogeneities and the inhomogeneous lattice strain are likely to increase phonon scattering. The size of the nanoclusters may also be important in making this scattering mechanism effective. The short-range nature of the local chemical ordering will broaden out Fermi-surface resonances shown to be important in thermopower enhancement⁶. Presumably, the size of the nanoclusters, their exact composition, the atomic ordering within them and their concentration with PbTe will be a sensitive function of the preparation conditions.

Adding Pb atoms in the minor phase greatly improves the result of the refinement. The reason is that Pb atomic number is much larger than the atomic numbers of Ag, Sb and Te and its scattering factor is quite different from those of the other three.

V. SUMMARY

In this structural study based on the PDF method, we verified that in the bulk material of $AgPb_mSbTe_{m+2}$, nanoclusters of a minor phase containing Ag, Pb, Sb and Te atoms form in the matrix of PbTe. We give evidence showing that the chemical composition of the minor phase is most likely between $AgPb_2SbTe_4$ and $AgPb_4SbTe_6$. We propose a structure for the minor phase based on PDF, TEM and theoretical considerations.

Acknowledgments

We would like to acknowledge help from Didier Wermeille, Doug Robinson, Pavol Juhas, Gianluca Paglia, Ahmad Masadeh, Hasan Yavas, HyunJeong Kim and Mouath G. Shatnawi in collecting data. We also thank S.D.Mahanti, Khang Hoang for helpful discussions. Work in the Billinge group was supported by the

NSF NIRT grant DMR-0304391. Work in the Kanatzidis group was supported by the ONR(MURI) program. Data were collected at the 6IDD beam-line Advanced Photon Source (APS). Use of the APS is supported by the U.S. DOE under Contract No. W-31-109-Eng-38. The MUCAT sector at the APS is supported by the U.S. DOE under Contract No. W-7405-Eng-82.

-
- * Electronic address: billinge@pa.msu.edu;
URL: <http://nirt.pa.msu.edu/>
- ¹ K. F. Hsu, S. Loo, F. Guo, W. Chen, J. S. Dyck, C. Uher, T. Hogan, E. K. Polychroniadis, and M. G. Kanatzidis, *science* **303**, 818 (2004).
 - ² $ZT = \sigma S^2 T / \kappa$, where T is the operating temperature of the device, S is the thermopower, and σ and κ are the electrical and thermal conductivities of the material, respectively.
 - ³ Z. H. Dughaish, *Physica B* **322**, 205 (2002).
 - ⁴ H. Beyer, J. Nurnus, H. Böttner, and A. Lambrecht, *Appl. Phys. Lett.* **80**, 1216 (2002).
 - ⁵ E. Quarez and K.-F. Hsu, *J. Am. Chem. Soc.* **127**, 9177 (2005).
 - ⁶ D. Bilc, S. D. Mahanti, E. Quarez, K.-F. Hsu, R. Pcionek, and M. G. Kanatzidis, *Phys. Rev. Lett.* **93**, 146403 (2004).
 - ⁷ T. E. Humphrey and H. Linke, *Phys. Rev. Lett.* **94**, 096601 (2005).
 - ⁸ G. D. Mahan and J. O. Sofo, *Proc. Nat. Acad. Sci. USA* **93**, 7436 (1996).
 - ⁹ T. Egami and S. J. L. Billinge, *Underneath the Bragg peaks: structural analysis of complex materials*, Pergamon Press, Elsevier, Oxford, England, 2003.
 - ¹⁰ S. J. L. Billinge and M. G. Kanatzidis, *Chem. Commun.*, 749 (2004).
 - ¹¹ S. Vensky, L. Kienle, R. E. Dinnebier, A. S. Masadeh, S. J. L. Billinge, and M. Jansen, *Z. Kristallogr.* **220**, 231 (2005).
 - ¹² P. J. Chupas, X. Qiu, J. C. Hanson, P. L. Lee, C. P. Grey, and S. J. L. Billinge, *J. Appl. Crystallogr.* **36**, 1342 (2003).
 - ¹³ A. P. Hammersley, ESRF Internal Report **ESRF98HA01T** (1998).
 - ¹⁴ X. Qiu, J. W. Thompson, and S. J. L. Billinge, *J. Appl. Crystallogr.* **37**, 678 (2004).
 - ¹⁵ S. J. L. Billinge, in *Local Structure from Diffraction*, edited by S. J. L. Billinge and M. F. Thorpe, page 137, New York, 1998, Plenum.
 - ¹⁶ H. M. Rietveld, *J. Appl. Crystallogr.* **2**, 65 (1969).
 - ¹⁷ J. Bloch, T. Proffen, and S. J. L. Billinge, PDFFIT2; an updated C++ implementation of the PDFFIT program, unpublished, 2005.
 - ¹⁸ Th. Proffen and S. J. L. Billinge, *J. Appl. Crystallogr.* **32**, 572 (1999).
 - ¹⁹ S. Geller and J. H. Wernick, *Acta Crystallogr.* **12**, 46 (1959).
 - ²⁰ K. Hoang, K. Desai, and S. D. Mahanti, *Phys. Rev. B* **72**, 064102 (2005).